Roadside Passive Multichannel Analysis of Surface Waves (MASW)

Choon B. Park[1] and Richard D. Miller[2]
[1]Park Seismic LLC, 2 Balsam Circle, Shelton, CT 06484
Email: choon@parkseismic.com
[2]Kansas Geological Survey, University of Kansas, 1930 Constant Avenue, Lawrence, Kansas 66047-3726
Email: rmiller@kgs.ku.edu

ABSTRACT

A 2-D receiver array, such as a cross or circular type, should be used in a passive surface wave survey to provide the most accurate results. It is often not possible to secure such a spacious area, however, especially if the survey has to take place in an urban area. A passive version of the multichannel analysis of surface waves (MASW) method is described that can be implemented with the conventional linear receiver array deployed alongside a road. Offline, instead of inline, nature of source points on the road is accounted for during dispersion analysis by scanning recorded wavefields through 180-deg azimuth range to separate wavefields from different azimuths and propagated with different phase velocities. Next, these wave fields are summed together along the azimuth axis to yield the azimuth-resolved phase velocity information for a given frequency. In addition, it is attempted to account for the cylindrical, instead of planar, nature of surface wave propagation that often occurs due to the proximity of source points, by considering the distance between a receiver and a possible source point. Performance of the processing schemes is compared to performance of the scheme that accounts for inline propagation only. Comparisons made with field data sets showed that the latter scheme resulted in overestimation of phase velocities up to 30 percent, whereas the overestimation could be reduced to less than 10 percent if these natures are accounted for according to the proposed schemes.

Introduction

The passive surface wave method is an alternative to the active survey method, which often does not achieve sufficient depth of investigation. In addition, as the necessity of surveys inside urban areas grows, utilizing surface waves generated by local traffic is deemed to be a fascinating choice (Asten, 1978; Louie, 2001; Okada, 2003; Suzuki and Hayashi, 2003; Yoon and Rix, 2004; Park *et al.*, 2004). Although this type of surface wave application had come under study nearly a half-century ago in Japan under the name of Microtremor Survey Method (MSM) (Aki, 1957; Tokimatsu *et al.*, 1992), it was not well known in Western countries until quite recently, with the exception of a few study groups (Asten, 1978; Asten and Henstridge, 1984). Spatial Autocorrelation (SPAC) (Aki, 1957) and f-k methods were commonly used to process passive surface waves for dispersion analysis. More recently, an imaging method similar to the one used in the active method was developed (Park *et al.*, 2004, 2007).

Because the true 2-D receiver array, such as a cross layout, is not a practical or possible mode of survey in urban areas populated with buildings, a method that can be implemented with the conventional 1-D linear receiver array deserves attention (Louie, 2001). The underlying assumption with a 1-D method lies in the nature of wave propagation, which is the same inline propagation as in the case of an active survey. Subsequent data processing for dispersion analysis is therefore a 1-D scheme considering only those waves propagating parallel to (inline with) the linear receiver line.

In the case of a passive survey alongside a road, points of surface wave generation are usually on the road since waves are generated when moving vehicles travel over irregularities in the road. Because the receiver line is always off the road, the wave propagation is rarely in accordance with the inline propagation, although approaching it when sources are at far distances. If strong waves from nearby source points dominate and their offline nature is not accounted for during the dispersion analysis, phase velocities are overestimated approximately in inverse proportion to the cosine of the azimuth ($\cos\theta$). Furthermore, considering relatively strong energy from nearby source points, the dominating mode of propagation may be not only offline but also cylindrical with a wavefront whose curvature cannot be ignored.

JEEG, March 2008, Volume 13, Issue 1, pp. 1–11

Methods to account for these offline and cylindrical characteristics are described, with results compared to those from a conventional analysis scheme based on inline plane wave propagation. Fundamentals of data acquisition and processing techniques have evolved from the multichannel analysis of surface waves (MASW) method (Park *et al.*, 1999) for active surface wave surveys. The offline nature is accounted for by a scheme (Park *et al.*, 2004) that scans through a possible range (180 deg) of incoming azimuths of dominating waves for each frequency component of the dispersion analysis. Next, all of the energy in this phase velocity-azimuth space is stacked (summed) along the azimuth (θ) axis to account for multiple energy peaks that may represent different modes and sources. The cylindrical nature was partially accounted for by an additional scheme that calculates the approximate distance between a specific receiver and a possible source point, which is determined from the consideration of azimuth and approximate distance between the receiver line and the road. It is shown that these proposed schemes can correct for the overestimation to some degree but not completely, indicating that a true 2-D array has to be used for the most accurate estimation. The incomplete correction becomes more significant for longer wavelengths. Tests with some field data sets show the overestimation caused by the conventional inline processing can be as large as 30 percent, whereas the overestimation can be reduced to less than 10 percent by using the proposed schemes.

Roadside Passive Surface Waves

Three different types of wave propagation can exist: inline plane (IP), offline plane (OP), and offline cylindrical (OC) propagations (Fig. 1). Propagation of waves generated from distant points on the surveying road (for example, at a distance 10 times or more the array length) can be an example of the IP type if the road is fairly straight in the corresponding segment (Fig. 1a). On the other hand, if the road turns or there are other roads around the surveying area, there can be waves generated at far distances approaching the receiver line with a significant azimuthal angle making an example of the OP type (Fig. 1b). Furthermore, source points on the surveying road can be close to the array (for example, at a distance shorter than a few times the array length from either end or even within the receiver line), which is an example of the OC type (Fig. 1c). Waves of OC type propagate into the receiver line with a significant curvature due to the proximity and the offline nature. A considerable amount of recorded energy can be of this origin due to the proximity of the major source points.

The IP waves will make a straight linear arrival pattern on the recorded data with a slope ($S = dt/dx$) the same as the inverse of the phase velocity ($1/c$) (*i.e.*, slowness) for a particular frequency (f) (Fig. 2). The OP waves will also make a straight linear arrival pattern, but with its slope always smaller than ($1/c$) of the IP case by a ratio of cosine of the azimuth ($\cos\theta$) (Park *et al.*, 2004). In this situation, its corresponding velocity (dx/dt) will be overestimated by a ratio of $1/\cos\theta$ if the offline nature is not properly accounted for. The arrival pattern of the OC waves will be hyperbolic with an asymptote the same as that of the OP for the same azimuth (θ).

Schemes for Dispersion Imaging

Dispersion imaging schemes to deal with each of these types of propagation are described. It is assumed that the road runs along the horizontal axis (x) with the receiver line parallel to it with a certain vertical separation (dy) (Fig. 3).

Inline Plane (IP) Waves

IP waves are the simplest type from the data processing perspective. They can be processed by any scheme commonly used for active surveys. The scheme by Park *et al.* (1998, 2004) calculates the relative energy, $E_{IP}(\omega,c)$, for a particular frequency ($\omega = 2\pi f$) and a scanning phase velocity (c) in the dispersion image. It first applies the necessary phase shift ($\phi_i = \omega x_i/c$) to the Fourier transformation, $R_i(\omega)$, of the *i-th* trace, $r_i(t)$, at offset x_i, next sums all (N) phase-shifted traces, and then takes the absolute value of the summed complex number:

$$E_{IP}(\omega, c) = \left|\sum_{i=1}^{N} e^{j\phi_i} R_i(\omega)\right| + \left|\sum_{i=1}^{N} e^{-j\phi_i} R_i(\omega)\right|. \quad (1)$$

To account for the possible bidirectional nature of the incoming waves from both ends of the receiver array, the step of phase shift followed by the summation is repeated by changing the sign of the phase shift in Eq. (1). A method by Louie (2001)–commonly known as the refraction microtremor (ReMi) method–is based on this algorithm by assuming that the major part of the recorded waves are of IP type and any other offline waves of significant energy, if they exist, should appear at higher phase velocities. It therefore tries to extract a curve by following a trend of lowest phase velocity in the energy band of dispersion in the space of $E_{IP}(\omega,c)$. With this method, however, consideration of the inherent banding effect due to the limited spatial coverage of the measurement is not properly accounted for.

Figure 4 shows processing results obtained by using Eq. (1) when applied to synthetic 24-channel records generated from an inline source (S0) (indicated in Fig. 3) and using the modeling scheme by Park and

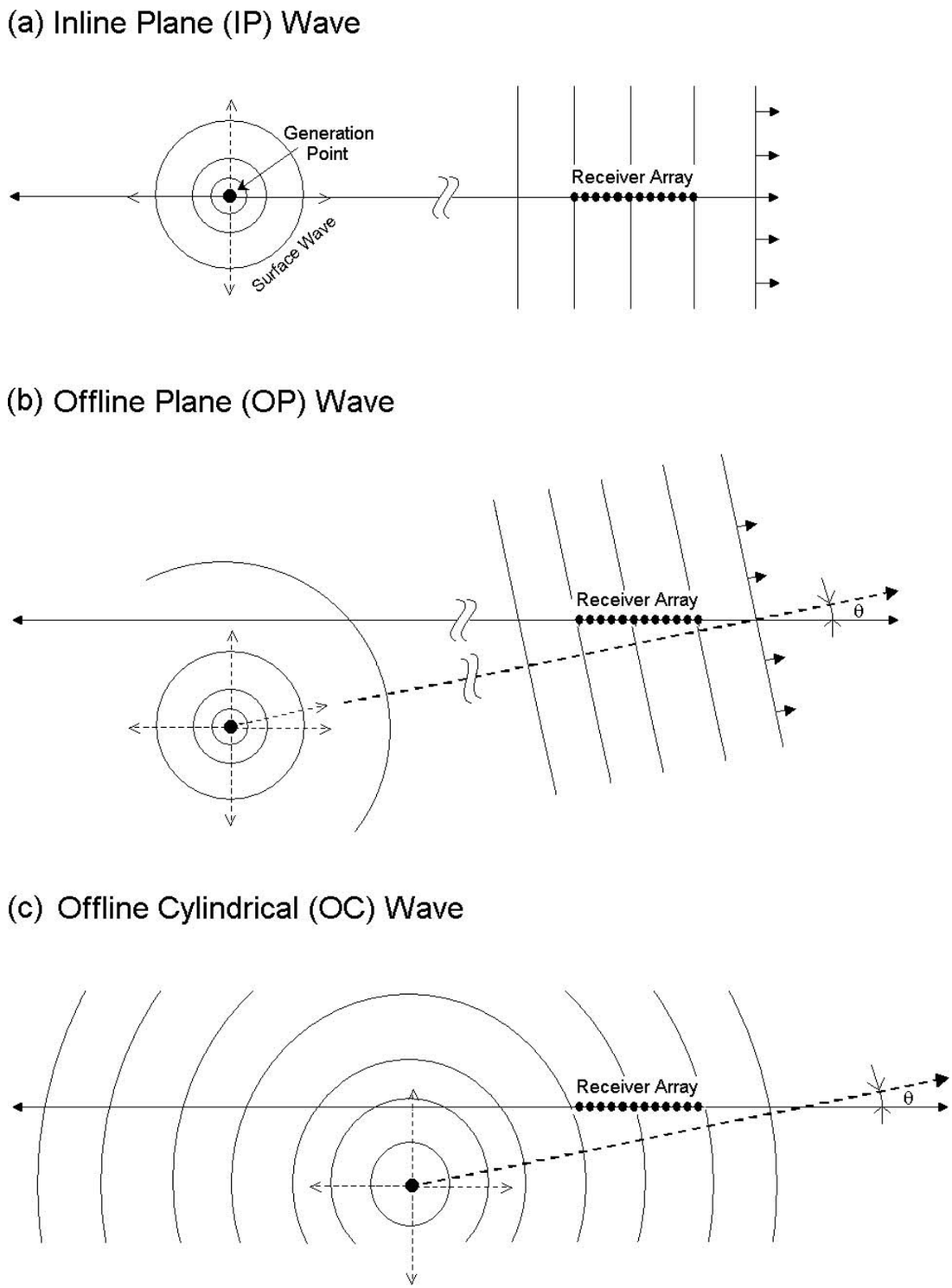

Figure 1. Three different types of possible wave propagation with a roadside surface wave method employing a 1-D linear receiver array parallel to road.

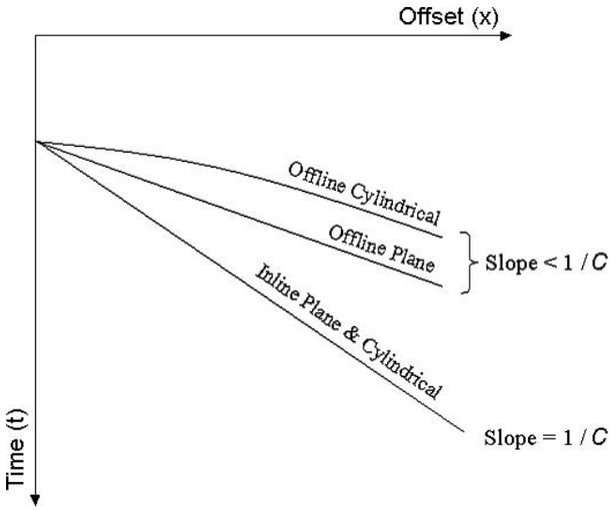

Figure 2. A schematic showing arrival patterns of different types of wave propagation as appearing in offset (*x*) and time (*t*) space.

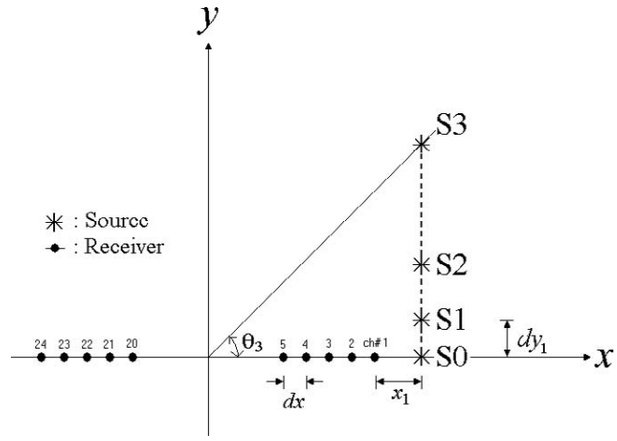

Figure 3. A relative coordinate system considering a linear receiver array and source points of different offline angles.

Miller (2005). A dispersion curve with an arbitrary constant phase velocity of 500 m/sec was used during the modeling. The effect of using different receiver array lengths is noticeable from the overall thickness of the banded (instead of thin-line) image changing with total length of the receiver line. Modeling the data with a perfectly inline source illustrates the inherent band appearance of the image resulting from a processing scheme applied to finite lengths in time (*t*) and space (*x*). Width of the band also changes with wavelength for a given length of the receiver line.

Offline Plane (OP) Waves

OP waves can be processed by any algorithm based on the conventional 2-D wavenumber (k_x-k_y) method (Lacoss *et al.*, 1969; Capon, 1969). The method by Park *et al.* (2004) modifies the traditional method in such a way that the possible multi-modal nature of dispersion can be

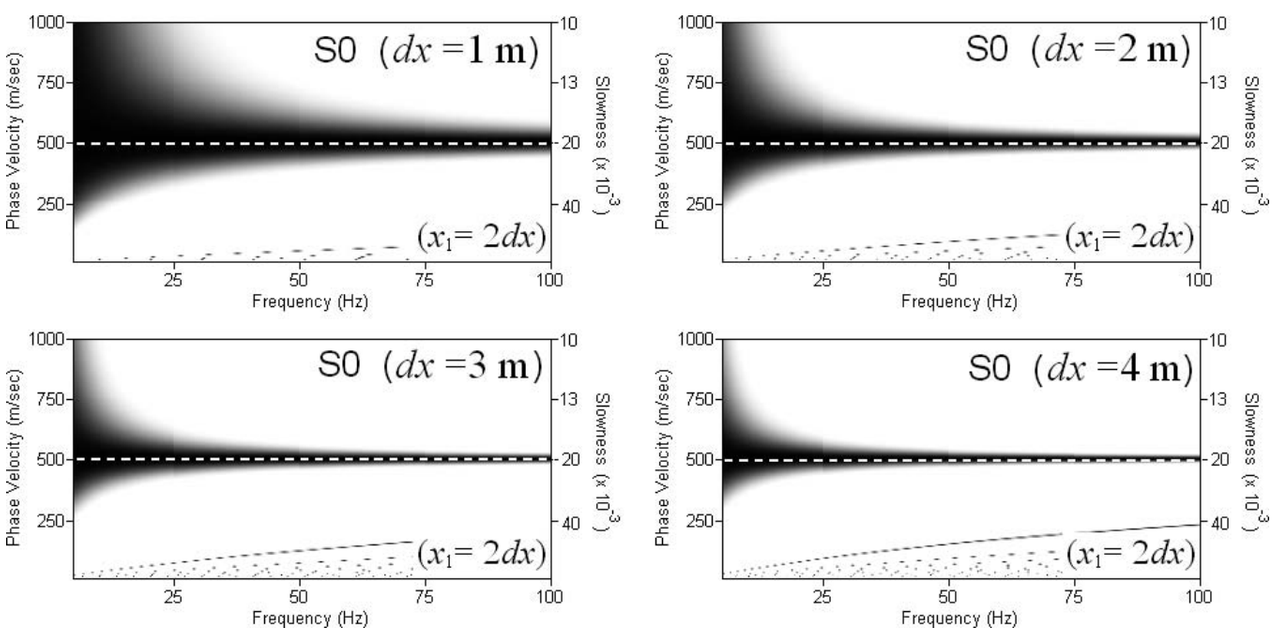

Figure 4. Dispersion images processed from synthetic records modeling a perfectly inline source (S0) in Fig. 3 obtained by using the IP wave processing scheme. Four different receiver intervals (*dx's*) were used in the modeling to consider different receiver array lengths.

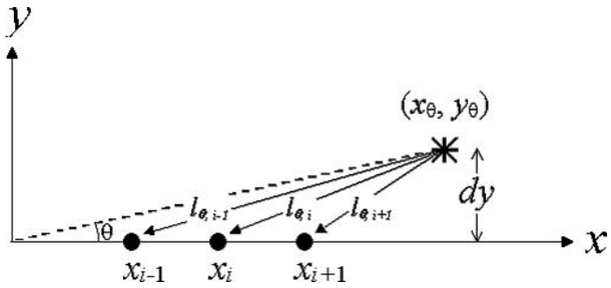

Figure 5. An illustration of how the offline cylindrical waves are accounted for during the scanning of an azimuth (θ).

imaged in an intuitive manner by stacking energy in the 2-D wavenumber space along the azimuth axis. This method (Park *et al.*, 2004) provides an additional parameter to be contrasted against the azimuthal (θ) dependence of incident seismic energy. For each frequency (ω), the energy, $E_{OP}(\omega,c,\theta)$, for a scanning phase velocity (c) is calculated by assuming an azimuth (θ). This calculation is then carried over the scanning range of the phase velocity (for example, 50 m/sec–3,000 m/sec with 5-m/sec increment), and then over that of the azimuth (for example, 0–180 deg in 5-deg increments):

$$E_{OP}(\omega, c, \theta) = \left| \sum_{i=1}^{N} e^{j\phi_{\theta,i}} R_i(\omega) \right| \text{ (for } 0^\circ \le \theta \le 180^\circ). \quad (2)$$

For a given c and θ, the necessary phase shift $\phi_{\theta,i} = -\omega x_i \cos\theta / c$ for a trace at x_i is calculated based on the projection principle (Park *et al.*, 2004). Here the scanning range of azimuth (θ) is only within the two quadrants (180 deg) due to the linear nature of the receiver line. All the IP waves that exist are handled in a correct manner as they are detected during the scanning of azimuth near 0 and 180 deg, respectively.

In the space of c and θ for a given ω, there can be multiple energy peaks occurring at different phase velocities and azimuths, representing different modes and sources, respectively. Also, different amplitudes of these peaks can represent different energy partitioning between modes or different strengths of the source or both. To fully account for all these possibilities, all the energy in c-θ space is stacked (summed) along the azimuth (θ) axis for N_θ different azimuths to produce $E_{OP}(\omega, c)$:

$$E_{OP}(\omega, c) = \sum_{i=1}^{N_\theta} E_{OP}(\omega, c, \theta_i) \quad (3)$$

that will constitute, in the final disperion-image space, one energy line at a particluar frequency, ω, showing the variation with different phase velocities.

Offline Cylindrical (OC) Waves

OC waves are processed in a similar manner to the OP waves using Eqs. (2) and (3), only with an additional consideration of the finite, rather than infinite, distance ($l_{\theta,i}$) between the source point (x_θ, y_θ) and each receiver

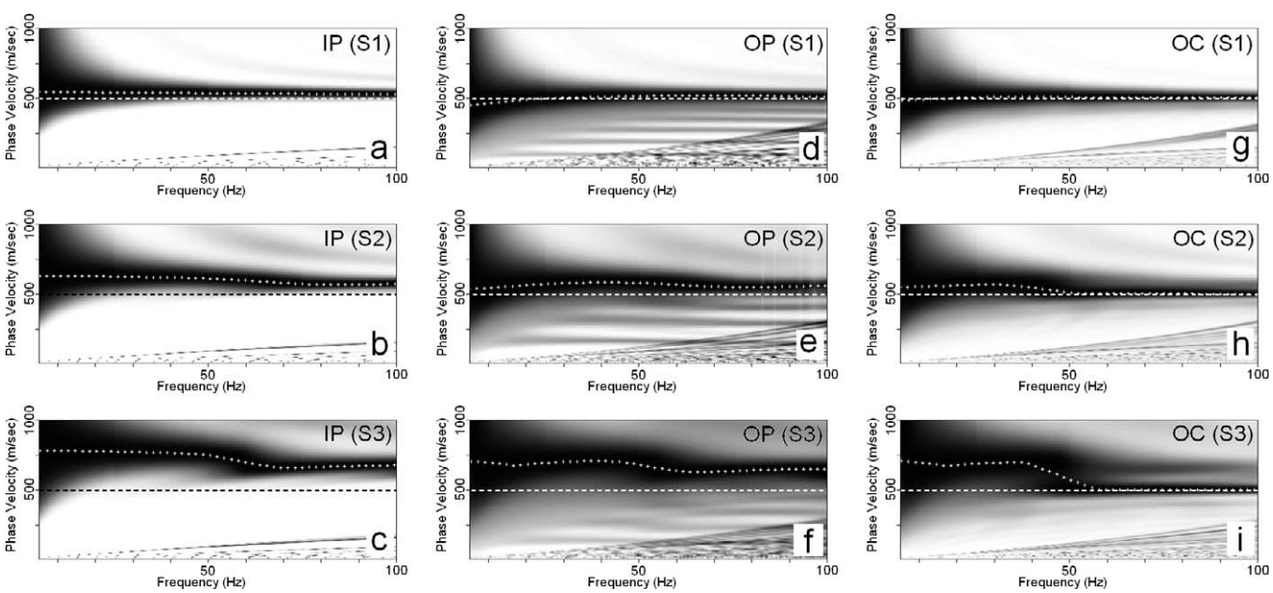

Figure 6. Dispersion images processed from synthetic records modeling three different offline sources (S1, S2, and S3) (marked in Fig. 3) by using three different processing schemes: IP, OP, and OC. The modeled phase velocity of 500 m/sec is indicated by a straight dotted line on each image, and trends of the energy peaks in each image are visible by cross marks superimposed on top of the major energy bands.

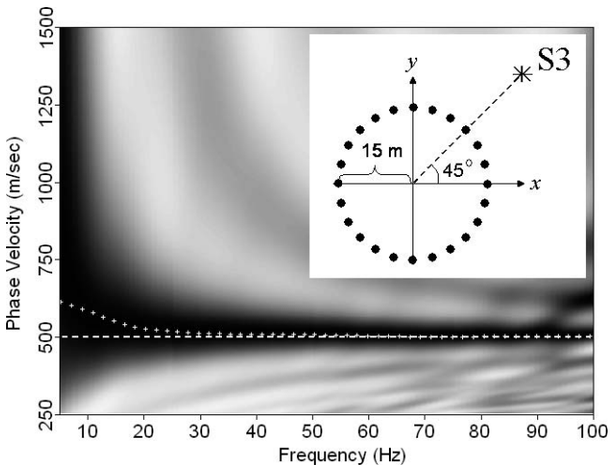

Figure 7. Dispersion image of the synthetic 24-channel record modeling the offline source S3 with a 2-D circular array (inset). The OP scheme was used to process the data.

point (x_i) for a scanning angle θ (Fig. 5):

$$l_{\theta,\,i} = \sqrt{(x_\theta - x_i)^2 + y_\theta^2} \text{ (with } x_\theta = y_\theta/\tan\theta \text{ and } y_\theta = dy). \quad (4)$$

Next, the phase shift term in Eq. (2) is determined as $\phi_{\theta,i} = -\omega l_{\theta,i/c}$. The distance, $l_{\theta,i}$, obviously can change as the road itself has its own width and irregularities may exist anywhere on the road. An extensive modeling experiment indicated that the exact distance, however, is not critical and that the distance between the center of the road and the receiver line is usually sufficient to account for the curvature in the arrival pattern of the OC waves. This scheme processes the IP waves correctly as it becomes identical to that for the IP waves for grazing azimuthal angles (close to 0 or 180 deg). OP waves (for example, waves from other nearby roads) can also be processed by this scheme, only with a slightly reduced sensitivity.

Synthetic Data Testing of Offline Schemes

Each of the three schemes was tested on synthetic data sets. A modeling scheme introduced in Park and

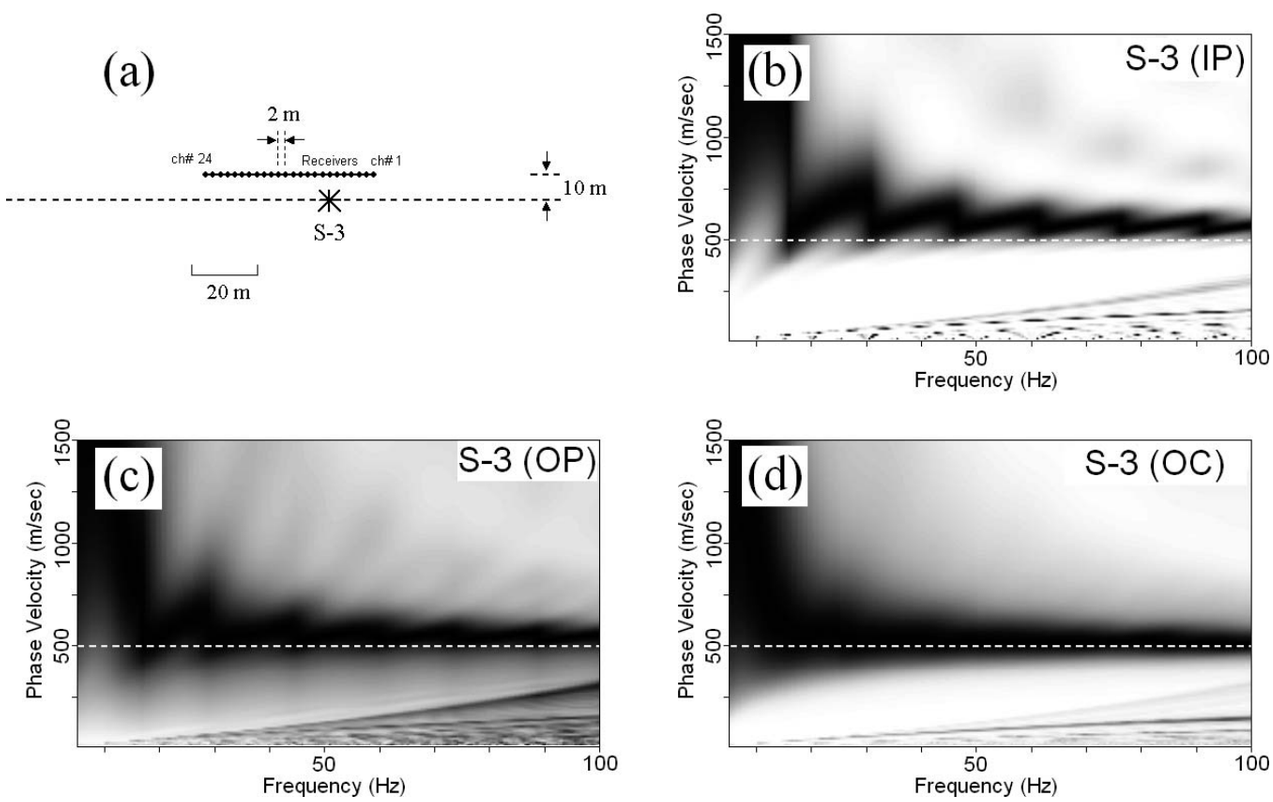

Figure 8. (a) A schematic showing the relative locations of the receiver array and an offline source (S-3) used to generate a 24-channel synthetic record. Dispersion images processed from the record by using (b) IP, (c) OP, and (d) OC schemes. 1

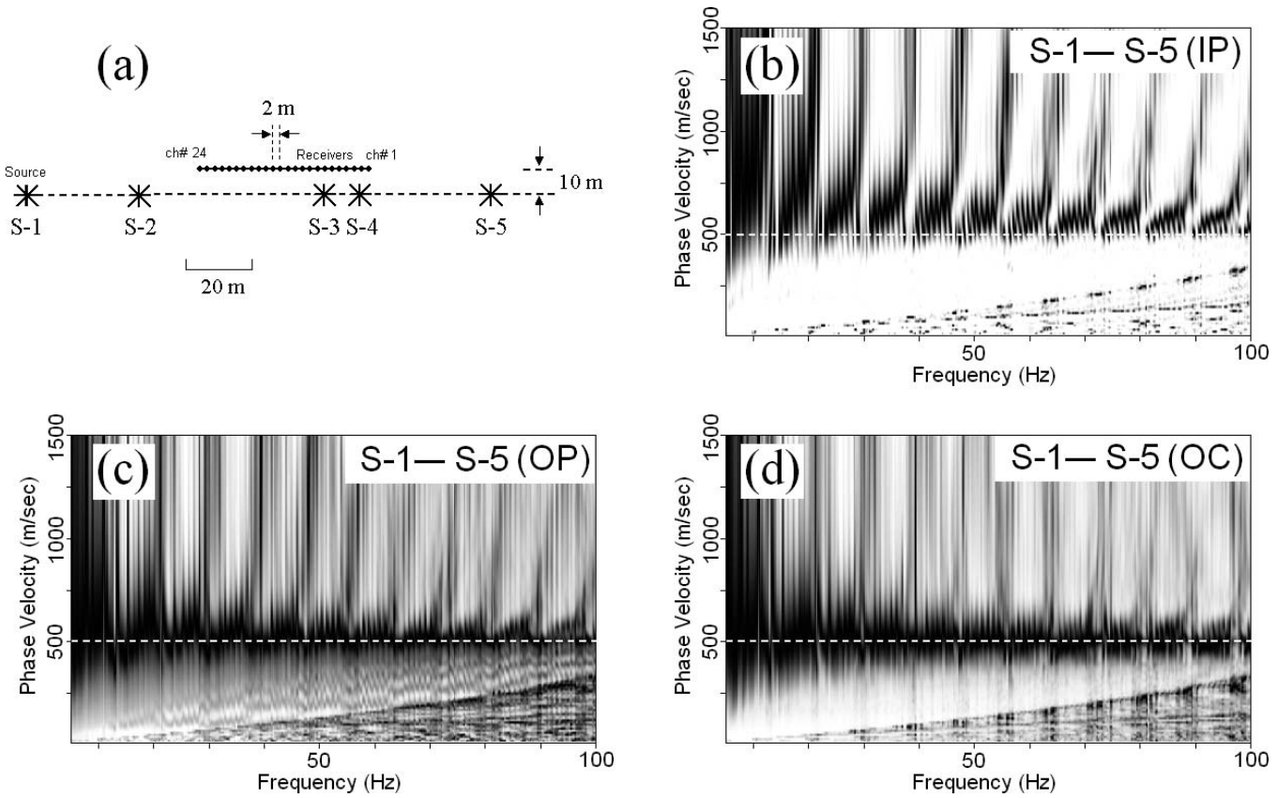

Figure 9. (a) A schematic showing relative locations of the receiver array and five offline sources (S-1 through S-5) simultaneously modeled to generate a synthetic 24-channel record. Dispersion images processed from the record by using (b) IP, (c) OP, and (d) OC schemes.

Miller (2005) was used to generate synthetic records (not shown) of 24-channel acquisition with a linear receiver array of 2-m spacing (Fig. 3). Summary of the modeling scheme is presented in the Appendix. Three different source points (S1, S2, and S3) were separately modeled, having azimuths of $\theta = 15°$, 30°, and 45° with the same inline offset of 4-m ($x_1 = 4$ m) and corresponding offline offsets (*dy*'s) of approximately 7 m, 15 m, and 27 m, respectively. A constant phase velocity of 500 m/sec was used for a frequency band of 5–100 Hz, giving an average wavelength (λ) of about 50 m. In addition to the cylindrical divergence term, attenuation of near-surface materials was accounted for by including a Q-factor of 30 as a frequency-dependent energy modulation factor of surface waves. Although all the modeled source points were offline, the inline processing scheme of Eq. (1) was also applied for comparison. Figure 6 shows processing results from each scheme. The modeled phase velocity of 500 m/sec is indicated by a straight dotted line in the figures. Those curves extracted from the amplitude peaks in the dispersion images also have been superimposed.

Results from the IP scheme show the imaged phase velocities being progressively higher as the azimuth of source point increases (Figs. 6a–6c). For relatively large azimuths ($\theta = 30°$ and 45°), the image trend converges to the theoretical value ($= c/\cos\theta$) at higher frequencies (for example, >50 Hz) where corresponding wavelengths become shorter than the offline offsets (*dy*'s), whereas it tends to deviate more at lower frequencies. This non-constant nature of the deviation is caused by the different degrees of proximity for different wavelengths (λ's) for a given offline offset (*dy*). Performance of the OP scheme (Figs. 6d–6f) shows a lesser degree of overestimation, indicating a correction capacity in comparison to the IP scheme. The results from the OC scheme (Figs. 6g–6i) generally show the least amount of overestimation for all three source points. None of the three schemes, however, shows complete results without any deviation from the correct value. The most accurate estimation is obtained through a survey using a true 2-D receiver array followed by data processing using the OP scheme (Fig. 7).

Relative performance of the OC scheme is maximized when the *x*-coordinate of an offline source point is within that of the receiver line (intra-line case), as noticed from another modeling example illustrated in Fig. 8. Figure 9 shows the performance results from a

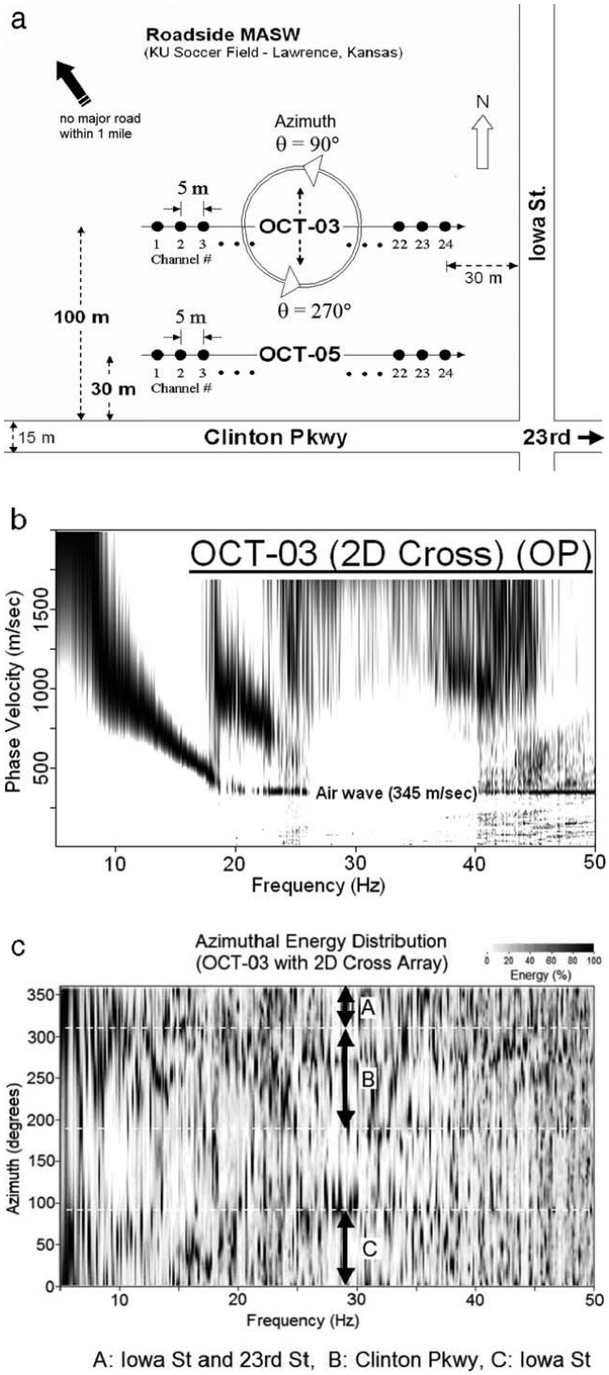

Figure 10. (a) Map showing field layouts for two experiments performed during October 2003 (OCT-03) and October 2005 (OCT-05). A 48-channel 2-D cross receiver array was used for the OCT-03. (b) Dispersion image processed from the 48-channel 2-D array records by using the OP scheme. (c) Azimuthal energy distribution for each frequency obtained during the dispersion processing.

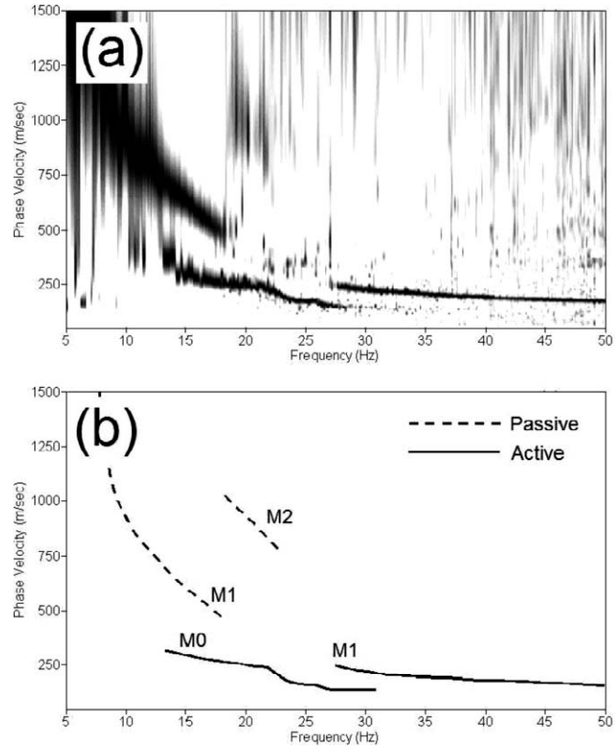

Figure 11. (a) Dispersion image constructed by combining active and passive dispersion image data sets together, and (b) modal interpretation of dispersion trends identified, from Park *et al.* (2005).

modeling of multiple source points with the same offline distance (*dy*) of 10 m. It is noted that the OC scheme gives the most accurate results with marginal improvement over the OP scheme, whereas results from the IP scheme, generally show the largest deviation trend of the image.

Field Data Example

Two sets of field data were used to test three processing schemes. One data set (OCT-03) was prepared from the data set acquired in October 2003 (Park *et al.*, 2004) near a soccer field in Lawrence, Kansas, by using a 2-D cross layout of 48 channels (Fig. 10) with a 5-m receiver spacing. The first 24-channel data that ran east-west (E-W) parallel to the Clinton Parkway were taken to mimic a 1-D linear array. The separation (*dy*) between this receiver line and the center of Clinton Parkway was about 100 m. For comparison purposes, a dispersion image that was obtained from the full data set of the 2-D cross layout is displayed in Fig. 10b. In addition, an azimuthal energy distribution, a by-product of the scheme by Park *et al.* (2004), is displayed in Fig. 10c that shows

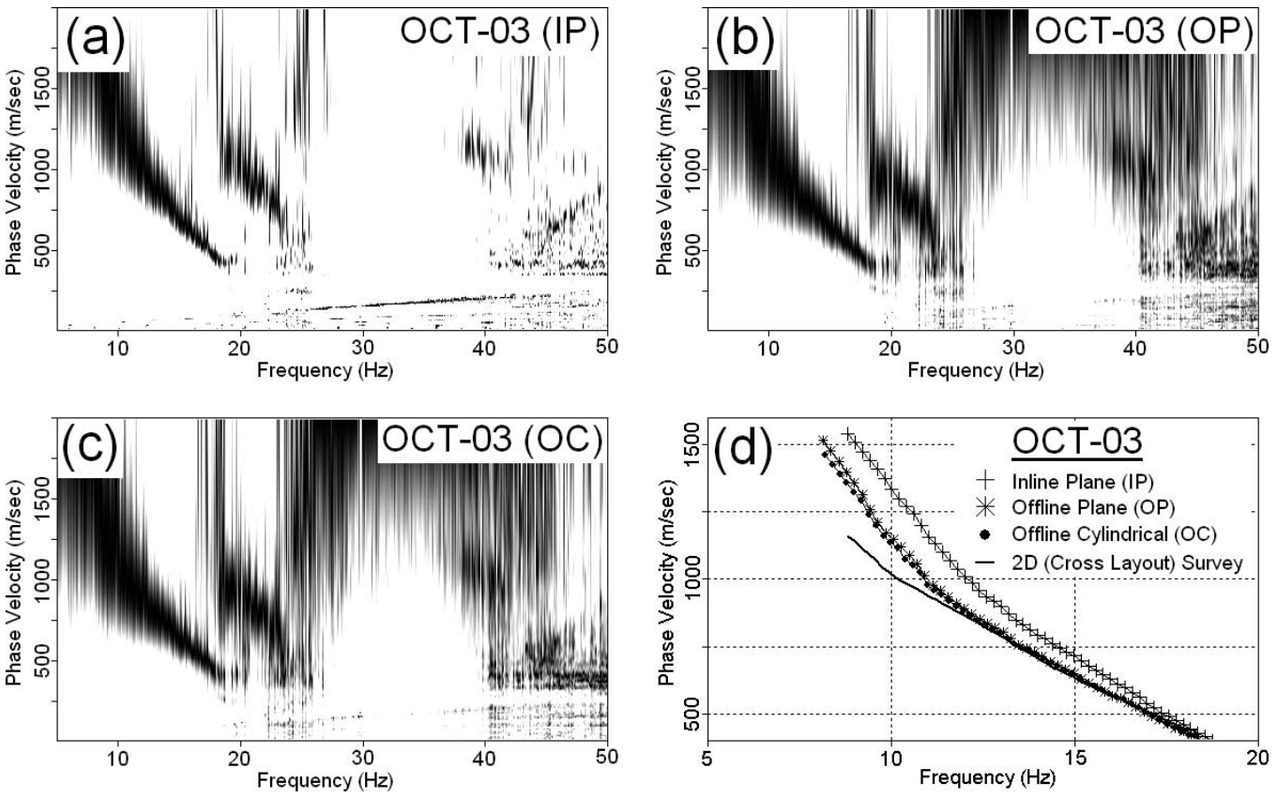

Figure 12. Dispersion images processed from 24-channel records along the E-W line used during the field experiment in October 2003, obtained by using (a) IP, (b) OP, (c) OC schemes, and (d) curves extracted from the major energy trend.

dominant azimuths for different frequencies analyzed for the image. The other set of data (OCT-05) was acquired in October 2005 using a 24-channel linear array directly south of the E-W line used for OCT-03 by using the same receiver spacing of 5 m (Fig. 10). This line was about 30-m from the road (dy = 30 m).

Ten individual records acquired at each survey time were processed using three different schemes, and their dispersion images were vertically stacked together (to increase the image resolution) to make the images displayed in Figs. 11 and 12. The strong major trend of dispersion visible on all images in 8–17 Hz was previously confirmed as a higher mode (M1), instead of the fundamental mode (M0), through a combined analysis with an active survey (Park *et al.*, 2005) (Fig. 11). Dispersion curves were extracted from the trends by picking maximum points in the energy band with a small interval (0.01 Hz) and then calculating the best fitting curve through the linear regression method. All curves are displayed in Figs. 12d and 13d. Curves from the IP scheme show overestimations in comparison to those from the other two schemes in both surveys. The amount of overestimation, however, becomes smaller as the receiver array gets closer to the road. It is also shown that the two offline (OP and OC) schemes resulted in a certain amount of overestimation for frequencies lower than 12 Hz (for wavelengths longer than about 75 m) as noticed when compared to the curve from the 2-D cross layout. Curves from the survey closer to the road (OCT-05) show a slight difference in general trend, possibly due to a slight difference in near-surface geology in comparison to the results from the previous survey performed about 70-m further away.

Discussion

It was shown through numerical modeling that the OC scheme should give a superior performance, especially when there are some intra-line source points on the road. Field data examples did not demonstrate this point, as the results from both OP and OC schemes were almost identical. This indicates that there were not strong intra-line source points on the road at the particular location where the surveys were performed. Azimuthal analysis for major source points in the surveyed area performed with the 2-D (cross and circular) receiver layouts (Park *et al.*, 2004; Park and Miller, 2005) indicated that major contribution of surface waves came from 23rd St., close to the intersection with Iowa St., as seen from Fig. 10c.

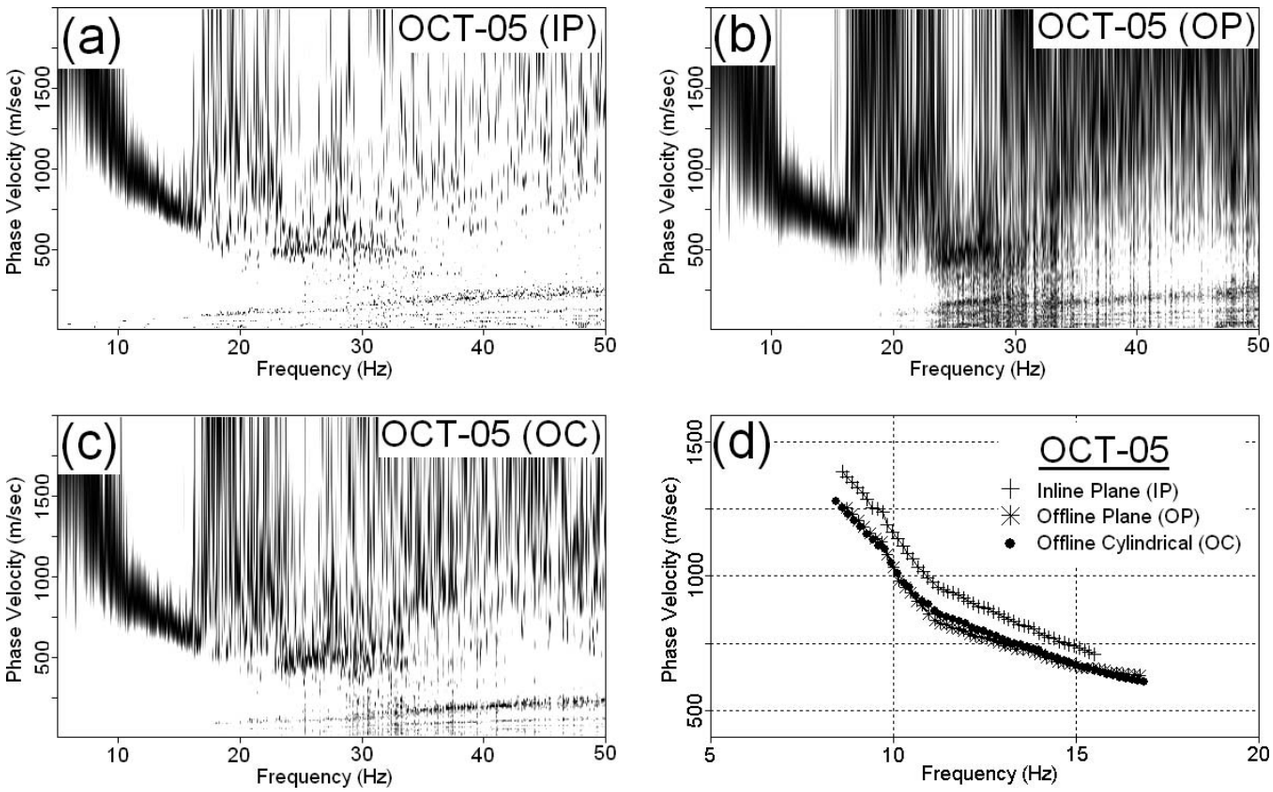

Figure 13. Dispersion images processed from 24-channel linear array used during the field experiment in October 2005, obtained by using (a) IP, (b) OP, (c) OC schemes, and (d) curves extracted from the major energy trend.

Although the theoretical analysis and modeling experiments indicated possible improvement of imaging quality with the OC scheme in comparison to the OP scheme, further comparative analysis is left for future research to better understand those influencing conditions not covered in this paper.

Even if a 2-D layout and the subsequent OP scheme are used, overestimation can still be significant for those long wavelengths comparable to distance to the major source points, as seen from the modeling result shown in Fig. 7. This finite (instead of infinite) nature of the source distance is inherent to the passive surface wave methods utilizing local traffic noise. The OC scheme was applied only to the linear array, but it can be extended to a 2-D layout.

Conclusions

When performing a roadside surface wave survey using a linear receiver array, a 2-D dispersion analysis scheme (despite the 1-D nature of data acquisition) that accounts for the offline nature of the passive surface waves is recommended. In addition, when using a relatively long receiver array with the possibility of strong surface waves being generated at nearby points on the road, accounting for the cylindrical nature through a simple modification of the 2-D algorithm appears to improve the accuracy of the processing.

Acknowledgments

Field experiments were made through careful preparations and precise operations performed by Brett Wedel, Noah Stimac, Larry Waldron, and Brett Bennett at the Kansas Geological Survey (KGS). We give our sincere appreciation to them. We also thank Marla Adkins-Heljeson and Mary Brohammer at KGS for their help with the manuscript preparation.

References

Aki, K., 1957, Space and time spectra of stationary stochastic waves, with special reference to micro-tremors: Bulletin Earthquake Research Inst., **35**, 415–456.

Asten, M.W., 1978, Geological control on the three-component spectra of Rayleigh-wave microseisms: Bulletin of the Seismological Society of America, **68**, 1623–1636.

Asten, M.W., and Henstridge, J.D., 1984, Array estimators and the use of microseisms for reconnaissance of sedimentary basins: Geophysics, **49**, 1828–1837.

Capon, J., 1969, High resolution frequency-wavenumber analysis: Proc. Inst. Elect. and Electron Eng., **57**, 1408–1418.

Lacoss, R.T., Kelly, E.J., and Toksöz, M.N., 1969, Estimation of seismic noise structure using arrays: Geophysics, **34**, 21–38.

Louie, J.N., 2001, Faster, better: Shear-wave velocity to 100 m depth from refraction microtremor arrays: Bulletin of the Seismological Society of America, **91**(2) 347–364.

Okada, H., 2003. The microtremor survey method: Geophysical Monograph Series, no. 12, Society of Exploration Geophysicists, Tulsa, OK.

Park, C.B., Miller, R.D., Xia, J., and Ivanov, J., 2007, Multichannel analysis of surface waves (MASW)−active and passive methods: The Leading Edge, **26**, 60–64.

Park, C.B., Miller, R.D., Ryden, N., Xia, J., and Ivanov, J., 2005, Combined use of active and passive surface waves: Journal of Engineering and Environmental Geophysics, **10**(3) 323–334.

Park, C.B., Miller, R.D., Laflen, D., Neb, C., Ivanov, J., Bennett, B., and Huggins, R., 2004, Imaging dispersion curves of passive surface waves: *in* Expanded Abstracts: 79th Annual International Meeting, Society of Exploration Geophysics, 1357–1360.

Park, C.B., and Miller, R.D., 2005, Multichannel analysis of passive surface waves – modeling and processing schemes: *in* Proceedings: ASCE/GeoInstitute Geo-Frontiers, 23–26.

Park, C.B., Miller, R.D., and Xia, J., 1999, Multichannel analysis of surface waves (MASW): Geophysics, **64**, 800–808.

Park, C.B., Xia, J., and Miller, R.D., 1998, Imaging dispersion curves of surface waves on multi-channel record: *in* Expanded Abstracts: 68th Annual International Meeting, Society of Exploration Geophysicists, 1377–1380.

Suzuki, H., and Hayashi, K., 2003, Shallow s-wave velocity sounding using the Microtremors array measurements and the surface wave method: *in* Proceedings: Symposium on the Application of Geophysics to Engineering and Environmental Problems, 1371–1376.

Tokimatsu, K., Shinzawa, K., and Kuwayama, S., 1992, Use of short-period microtremos for vs profiling: Journal of Geotechnical Engineering, **118**(10) 1544–1558.

Yoon, S., and Rix, G., 2004, Combined active-passive surface wave measurements for near-surface site characterization: *in* Proceedings: Symposium on the Aplication of Geophysics to Engineering and Environmental Problems, 1556–1564.

APPENDIX
MODELING SCHEME FOR PASSIVE SURFACE WAVES

The following scheme generates a synthetic seismogram of surface waves from given dispersion curve(s) and source-receiver location information. It is not a modeling scheme starting from a layered earth model. Its main utility is to test a dispersion analysis scheme to be used for processing passive surface waves. It calculates arrival times of all the frequencies being considered at each receiver location. Geometric (cylindrical) damping and attenuation (Q-factor) effects are taken into account as an amplitude-modulation factor. In the case of multiple sources and modes, the same calculation is repeated independently for each source and each mode, and then individual results are vertically stacked together to constitute the final seismogram (seismic trace).

It is assumed that, for a frequency ω, an arbitrary (k-th) source, $S_k{}^m(\omega)$, of passive surface waves has arbitrary location, $L_k = \{x_k, y_k\}$, amplitude, $a_k{}^m$, phase delay, δ_k, and mode number, m, to be represented in frequency domain as

$$S_k{}^m(\omega) = a_k{}^m \exp\{-j(\omega + \delta_k)\}. \tag{1}$$

The phase delay, δ_k, accounts for an arbitrary excitation time of the source. Next, its signature, $R_i^{m,k}(\omega)$, on an arbitrary (i-th) receiver at $L_i = \{x_i, y_i\}$ is determined after two modulation factors (amplitude, $A_{ik}{}^m$, and phase, $P_{ik}{}^m$) are applied to the above expression (1):

$$R_i^{m,\,k}(\omega) = A_{ik}{}^m P_{ik}{}^m S_k{}^m(\omega) \tag{2}$$

where

$$A_{ik}^m = \exp(\alpha l_{ik})/l_{ik},\ P_{ik}{}^m = \exp\left(j\omega l_{ik}/c_\omega{}^m\right),$$

$$\alpha = \text{attenuation coefficient} = \omega/(c_\omega{}^m Q),$$

Q = the quality factor, $c_\omega{}^m$ = phase velocity of $m-th$ mode for frequency ω, and

$$l_{ik} = \sqrt{(x_i - x_k)^2 + (y_i - y_k)^2}.$$

Therefore, when multiple modes are generated by the k-th source, the resultant multi-modal surface waves at i-th receiver, $R_i^k(\omega)$, are determined by summing over all modes:

$$R_i{}^k(\omega) = \sum_{m=0}^{M} R_i^{m,\,k}(\omega) \quad (\text{total M} + 1 \text{ modes}). \tag{3}$$

In the same way, if multiple sources are involved, then the summation is also carried over all sources:

$$R_i(\omega) = \sum_{k=1}^{k} R_i^k(\omega) \quad (\text{total } K \text{ sources}). \tag{4}$$

Lastly, the synthetic seismogram, $r_i(t)$, for (i-th) receiver is obtained from the inverse Fourier transformation of $R_i(\omega)$:

$$r_i(t) = \text{FFT}^{-1}\,[R_i(\omega)]. \tag{5}$$

Authors Queries

Journal: **Journal of Environmental and Engineering Geophysics**
Paper: **eego-13-01-01**
Title: **Roadside Passive Multichannel Analysis of Surface Waves (MASW)**

Dear Author
During the preparation of your manuscript for publication, the questions listed below have arisen. Please attend to these matters and return this form with your proof. Many thanks for your assistance

Query Reference	Query	Remarks
1	Author: Sometimes a hyphen is used in offline sources (ex. "S-3"; see Figs. 8 and 9) and sometimes not (ex. S3; see Figs. 6 and 7). Are both correct? Proofreader	